Japanese Journal of Applied Physics **56**, 06GM01 (2017)
https://doi.org/10.7567/JJAP.56.06GM01

REGULAR PAPER

Numerical investigation of perforated polymer microcantilever sensor for contractile behavior of cardiomyocytes

Trieu Khoa Nguyen[1], Dong-Weon Lee[2], and Bong-Kee Lee[2*]

[1]*Graduate School of Mechanical Engineering, Chonnam National University, Gwangju 61186, Republic of Korea*
[2]*School of Mechanical Engineering, Chonnam National University, Gwangju 61186, Republic of Korea*

*E-mail: b.lee@chonnam.ac.kr

Received November 30, 2016; accepted February 21, 2017; published online May 15, 2017

In this study, a numerical investigation of microcantilever sensors for detecting the contractile behavior of cardiomyocytes (CMs) was performed. Recently, a novel surface-patterned perforated SU-8 microcantilever sensor has been developed for the preliminary screening of cardiac toxicity. From the contractile motion of the CMs cultured on the microcantilever surface, a macroscopic bending of the microcantilever was obtained, which is considered to reflect a physiological change. As a continuation of the previous research, a novel numerical method based on a surface traction model was proposed and verified to further understand the bending behavior of the microcantilevers. Effects of various factors, including surface traction magnitude, focal area of CMs, and stiffness of microcantilever, on the bending displacement were investigated. From static and transient analyses, the focal area was found to be the most crucial factor. In addition, the current result can provide a design guideline for various micromechanical devices based on the same principle.

1. Introduction

The quantitative analysis of the physiological responses of cardiomyocytes (CMs) is important for achieving a stable cell culture as well as for understanding the mechanism of heart failure.[1–3] Their autonomous motion of periodical beating has also been attracting more attention, thereby being employed in developing new microsystems and/or in understanding the biochemical effects of several drugs.[2,4–6] Particularly for the investigation of the biochemical effects, simple polymeric structures such as micropost[5,7] or microcantilever[8,9] have been commonly utilized because a change in the physiology of the CM's contraction force produces a macroscopic behavior of these structures. The micropost or micropillar method optically measures the deflection, which is then translated into the corresponding contraction force using a well-known beam-bending theory.[10,11] However, because it requires a post-analysis of optical microscopy images,[12–14] a real-time analysis cannot be easily achieved. In addition, because there exist different effects of cell adhesion and locomotion compared with a typical flat surface, the reliability of the obtained experimental result is insufficient together with a relatively small displacement from a single-cell level.[15] In contrast, the cantilever method measures a macroscopic bending of the microcantilever, which is caused by a contractile behavior of the CMs in three-dimensional structure with reconstituted cell-to-cell connections and synchronized tissue-like behavior.[16,17] In this manner, it can usually yield a larger displacement with an improved ease of use. Like the micropost method, it shows difficulties in a real-time measurement because of the post-analysis of optical images. Even though impedance sensor arrays are also valuable candidates for high-throughput drug screening, it was reported that there exists a potential of unwanted side effects due to the current flow.[18–20]

To overcome the drawbacks of the previous techniques, a novel SU-8 microcantilever sensor to characterize the contractile behavior of CMs in vitro has recently been developed.[21] This cantilever-based measurement system including a laser vibrometer and a micro-motorized stage was built to measure the changes in contraction force during the cell culture period. In addition, it was a fast and real-time measurement so that the effects of drugs on contraction force and beating frequency could be timely and precisely analyzed.

However, the microcantilever was designed and produced to have holes for the easy lift-off from the substrate during the fabrication step. As any geometrical change in the microcantilever structure can affect its performance, the influence of holes should be investigated to achieve a more precise sensing output. Furthermore, although there have been several developments of micromechanical devices utilizing the autonomous motion of CMs, the relationship between the CMs' contractile motion and the resultant macroscopic behavior of the micro-mechanical device was not clearly investigated. It is also required to establish a guideline of designing other microdevices based on the same principle.

In this study, we present a numerical investigation to analyze the bending characteristic of the perforated SU-8 microcantilever. To treat the surface traction induced by the CMs, a simple numerical model was proposed and used to impose the boundary conditions. The effects of surface traction magnitude and focal area of the CMs on the mechanical response of the microcantilevers were investigated. The stiffness of the perforated microcantilever was analyzed to elucidate the effect of holes on the macroscopic bending motion. The transient analysis based on the time-varying surface traction was also carried out to verify the usefulness of the current numerical model.

2. Numerical method

In this study, a numerical analysis was performed using a commercial software (COMSOL Multiphysics®), which was developed on the basis of a finite element method. To consider both static and transient situations, a linear elastic model of Navier's equation [as indicated in Eq. (1)] was solved.

$$\rho \frac{\partial^2 u}{\partial t^2} = \nabla \cdot \sigma + F_v \tag{1}$$

In Eq. (1), u, σ, and F_v represent displacement field, stress tensor, and body force, respectively.

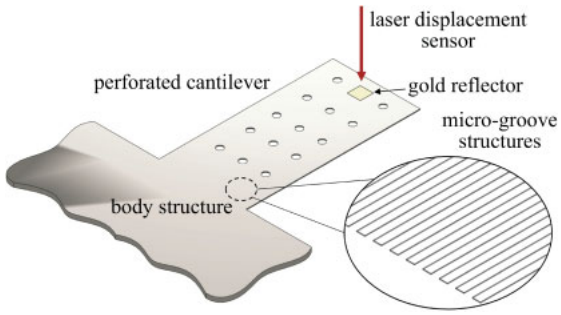

Fig. 1. (Color online) Schematic diagram of the perforated microcantilever sensor investigated in this study.

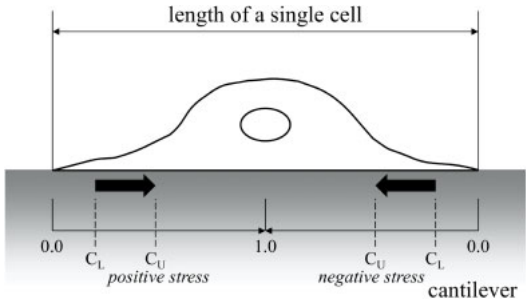

Fig. 2. (Color online) Proposed surface traction model with two parameters to describe the contraction force within a single cell.

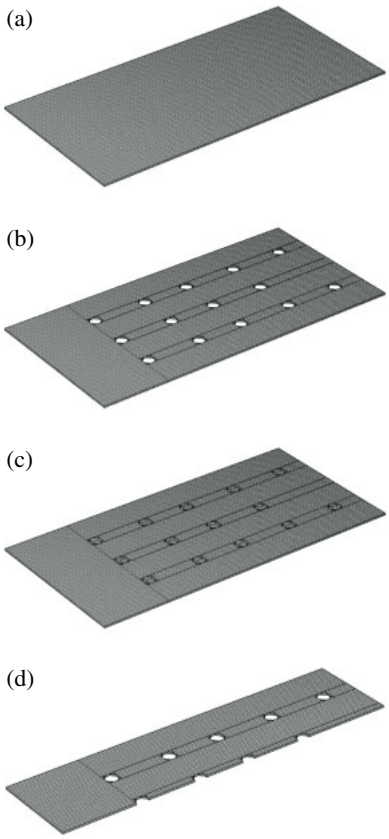

Fig. 3. (Color online) Finite element meshes used in the present study: (a) plain microcantilever, (b) perforated microcantilever, (c) plain microcantilever with confined cells for the comparative study, and (d) half model of the perforated microcantilever for the transient analysis.

Figure 1 illustrates the three-dimensional geometrical model of the previously developed microcantilever sensor.[21] It basically consisted of body structure and microcantilever whose width, length, and thickness were 2 mm, 4 mm, and 20 μm, respectively. On the top surface of the microcantilever where CMs were cultured, longitudinal microgroove structures of 0.8 μm depth and 3 μm width were formed. Note that the micro-groove structures in the longitudinal direction could produce the accumulated action of the cultured CMs, thereby enhancing the macroscopic bending motion of the microcantilever. The bending motion was detected by the external laser displacement sensor in real time.

To implement the surface traction on the top surface as the boundary condition, a simple numerical model was proposed as shown in Fig. 2. This model assumes that there exists only a shear component of the surface traction. The surface traction is also assumed to be parallel to the longitudinal direction of the microcantilever due to the perfectly aligned CMs. It is worth noting that the forces in other directions were considered to have little effect on the vertical bending of the microcantilever.[2,22] Two parameters of C_L and C_U represent lower and upper bounds of the focal area, respectively. The areas defined by C_L and C_U are the effective areas for positive and negative surface tractions within a single cell, generating the compressive stress only on the top surface. By controlling these parameters, the effect of focal area on the bending motion could be easily investigated. In this study, the constant surface traction within the focal area was assumed. Because the magnitude of the surface traction was reported as 2–5 nN/μm^2 for typical CMs,[23] the values of the suggested range were investigated.

Figure 3 shows the finite element meshes of the microcantilever structures. Figures 3(a) and 3(b) represent plain and perforated microcantilevers, respectively. To investigate the correlation between stiffness and surface traction area, a comparative model [Fig. 3(c)] was also prepared. It was designed to have the same geometry as the plain microcantilever, resulting in the same mechanical stiffness. However, some areas corresponding to holes in the perforated microcantilever were assumed to have no surface traction. In this manner, the comparative study could be carried out. For the transient analysis, only half of the geometrical model was used to minimize the required computational cost. Figure 3(d) shows the half model of the perforated microcantilever as one example.

The left-hand-side surface among the six planes of the geometrical model was assumed to be connected to the body structure. The fixed boundary condition, where there is no displacement, was assigned only on this plane. The top surface was exposed to the periodic surface traction based on the proposed model. Four other planes were treated as the free surface.

3. Results and discussion

3.1 Bending displacement of microcantilever sensors

The static numerical analysis of the microcantilevers was carried out to verify the current model and to investigate the effect of holes embedded in the perforated microcantilever on the bending displacement. Three finite element models, namely, plain [Fig. 3(a)], perforated [Fig. 3(b)], and comparative microcantilevers [Fig. 3(c)], were used. For all cases, the constant magnitude of surface traction was assumed to be 5 nN/μm^2. Two parameters for the surface

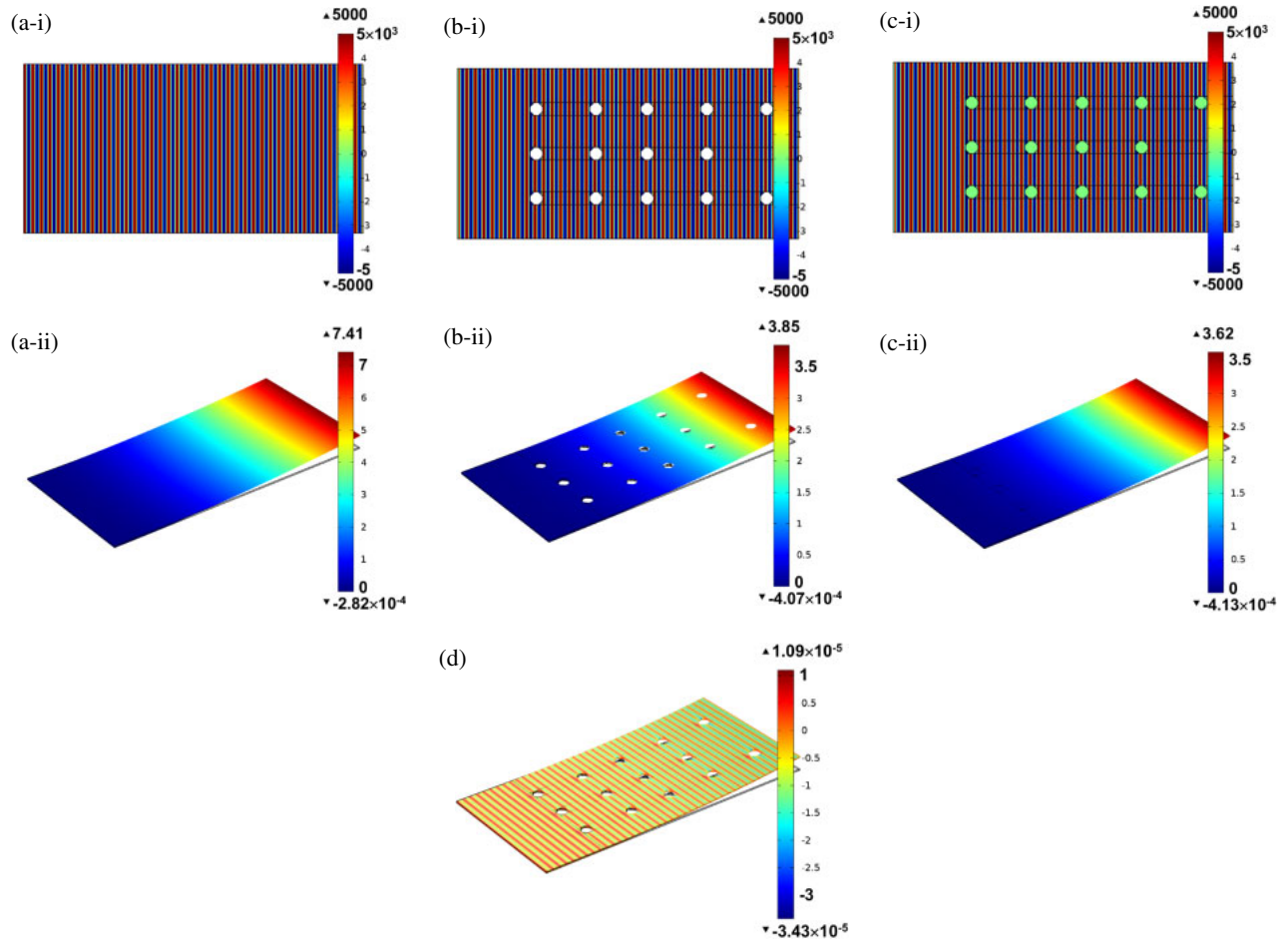

Fig. 4. (Color online) Representative numerical results of the static analysis: (a) surface traction distribution (with a dimension of N/m^2, which corresponds to $10^3\,nN/\mu m^2$) and bending displacement of the plain model (with a dimension of μm), (b) those of the perforated model, (c) those of the comparative model, and (d) effective strain distribution of the perforated microcantilever.

traction model, C_L and C_U, were chosen as 0.0 and 1.0, respectively. It was reported that the typical length of a single CM varies from 62.9 to 112.05 μm depending on cell type and measurement method.[24–29] In this study, a length of 100 μm was assumed for the sake of simplicity in imposing the periodic surface traction as the boundary condition. Young's modulus and Poisson's ratio for the microcantilever material were assumed to be 2 GPa and 0.22, respectively.[30]

Figure 4 shows the representative results from the static analysis under the prescribed conditions. As shown in Figs. 4(a-i), 4(b-i), and 4(c-i), the periodic surface traction was properly assigned with the maximum and minimum values of 5 and $-5\,nN/\mu m^2$, respectively. Note that for the comparative model [Fig. 4(c-i)], the areas corresponding to holes in the perforated microcantilever were excluded from the periodic surface traction. Because the periodic contractile surface traction was assigned only on the top surface, the asymmetric deformation of the microcantilever was produced, consequently resulting in the upward bending motion. The bending behaviors of the investigated models are shown in Figs. 4(a-ii), 4(b-ii), and 4(c-ii). The maximum displacement, which was observed at the free edge, for each model is summarized in Table I. As listed, it was predicted that the maximum bending displacement of the perforated microcantilever was reduced to around 48% compared with the plain one even though only 3% of the total area exposed to the surface traction was reduced. The total amount of the surface traction from the cultured CMs was found to show a larger effect on the macroscopic bending motion than the mechanical stiffness of the microcantilever. This effect could be confirmed from the comparative model, which was constructed to have the same stiffness as the plain microcantilever. On the other hand, the surface area exposed to the periodic traction was equal to that of the perforated microcantilever. As shown in Fig. 4(c-ii), the comparative model showed the reduced displacement, which was similar to that of the perforated microcantilever. Note that from the viewpoints of bending direction and magnitude, the present numerical results agreed well with the real experiment.[21]

Table I. Maximum displacement for each case.

Model type	Displacement (μm)	Relative reduction (%)
Plain microcantilever	7.414	—
Perforated microcantilever	3.847	48.112
Comparative model	3.619	51.187

Figure 4(d) shows the effective strain distribution of the perforated microcantilever as the representative example. The maximum strain appeared over the top surface in a periodic manner owing to the compressive surface traction within a single cell area. The level of the maximum strain was about 10^{-5}, which is within the linear range of the typical SU-8.[31]

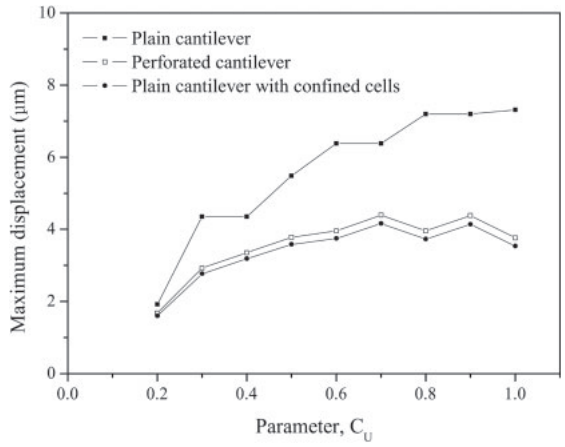

Fig. 5. Effect of model parameter C_U on the maximum bending displacement (for the case of constant $C_L = 0.0$ and $E = 2$ GPa).

Therefore, a linear elastic analysis in this study can be considered as the suitable approach.

3.2 Effects of focal area and stiffness

As discussed earlier, the total area exposed to the surface traction showed more effect on the macroscopic bending behavior of the microcantilever. To continue the investigation further, the effect of focal area on the bending displacement was examined on the basis of three microcantilever models. In the current surface traction model, the two parameters C_L and C_U define the focal area. While C_L was kept at 0.0, C_U was increased from 0.2 to 1.0 with intervals of 0.1. Because the increase in C_U represents the enlarged focal area, the effect of focal area on the bending behavior can be investigated in this way. It is worth noting that the controllable focal area is an advantage of the current surface traction model over the previously employed methods for the contractile forces.[2,15,31]

The maximum displacements of the bent microcantilevers are shown in Fig. 5. As the total amount of contractile force increases with increasing C_U, the resultant bending displacement was found to increase for all cases. Note that the Stoney formula, which has been commonly employed to estimate the surface stress of a thin film, a cell, or a biomolecule on one surface of the substrate, predicts a linear increase in the maximum bending displacement with increasing surface traction.[32] However, in the Stoney formula, it was assumed that the surface stress is equally distributed over the entire surface, which is quite different from the present case. The different distribution of the surface traction can be considered to be a reason for the current asymptotic change in the maximum bending displacement, like in the case of patterned films on the substrate.[33] In addition, the maximum displacement of the perforated microcantilever was always lower than that of the plain one. Note that the slight decrease in the displacement came from the numerical mismatch between the length of the cell and the area of holes in the perforated microcantilever when C_U exceeded 0.8. In this regard, the same trend was also found in the case of the comparative model.

The perforated microcantilever had a lower stiffness due to the holes in the body. To investigate the stiffness effect, two simple approaches were carried out. The stiffness of the cantilever structures was calculated using (1) Hooke's law on the basis of a static structural analysis assuming a simple line force along one side edge and (2) effective mass based on a dynamic structural analysis of natural frequency.[34,35] Table II lists the calculated stiffness values. In the case of the perforated microcantilever, the loss of mass in the body resulted in a decreased stiffness. Note that the stiffness of the plain microcantilever calculated using a well-known Euler–Bernoulli equation was 0.125 N/m, which is the same as the stiffness calculated by the effective mass method. In this regard, the perforated microcantilever tended to show a slightly larger bending displacement under the same surface traction condition (comparative model case). However, compared with the plain microcantilever, the perforated one showed the decreased bending displacement despite the lowered stiffness. It means that the surface traction or the amount of the contractile force of CMs cultured on the surface is the most crucial factor for the macroscopic bending deformation of the microcantilever sensor.

Table II. Calculated stiffness of the microcantilever structures (in N/m).

Simulation model	Hooke's law	Effective mass method
Plain microcantilever	0.128	0.125
Perforated microcantilever	0.122	0.108

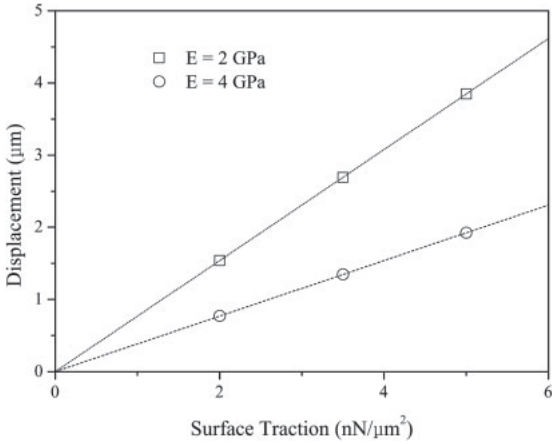

Fig. 6. Effect of magnitude of surface traction and Young's modulus on the bending displacement in the perforated microcantilever.

3.3 Effects of surface traction magnitude and Young's modulus

To validate the current numerical method, the effects of the magnitude of the surface traction and Young's modulus of the microcantilever material were investigated. As discussed, the surface traction of the typical CMs varies from 2–5 nN/μm^2. Moreover, Young's modulus of the cured SU-8 usually ranges from 2 to 4 GPa. In this regard, three levels of the surface traction magnitude (i.e., 2, 3.5, and 5 nN/μm^2) and two levels of Young's modulus (i.e., 2 and 4 GPa) were chosen. By changing these parameters, the maximum displacement of the perforated microcantilever was calculated.

Figure 6 shows the relationship between the magnitude of the surface traction and the maximum displacement of the perforated microcantilever with respect to two distinct Young's moduli. The maximum displacement was linearly proportional to the surface traction. It can be easily expected from a linear elastic theory used in the current numerical

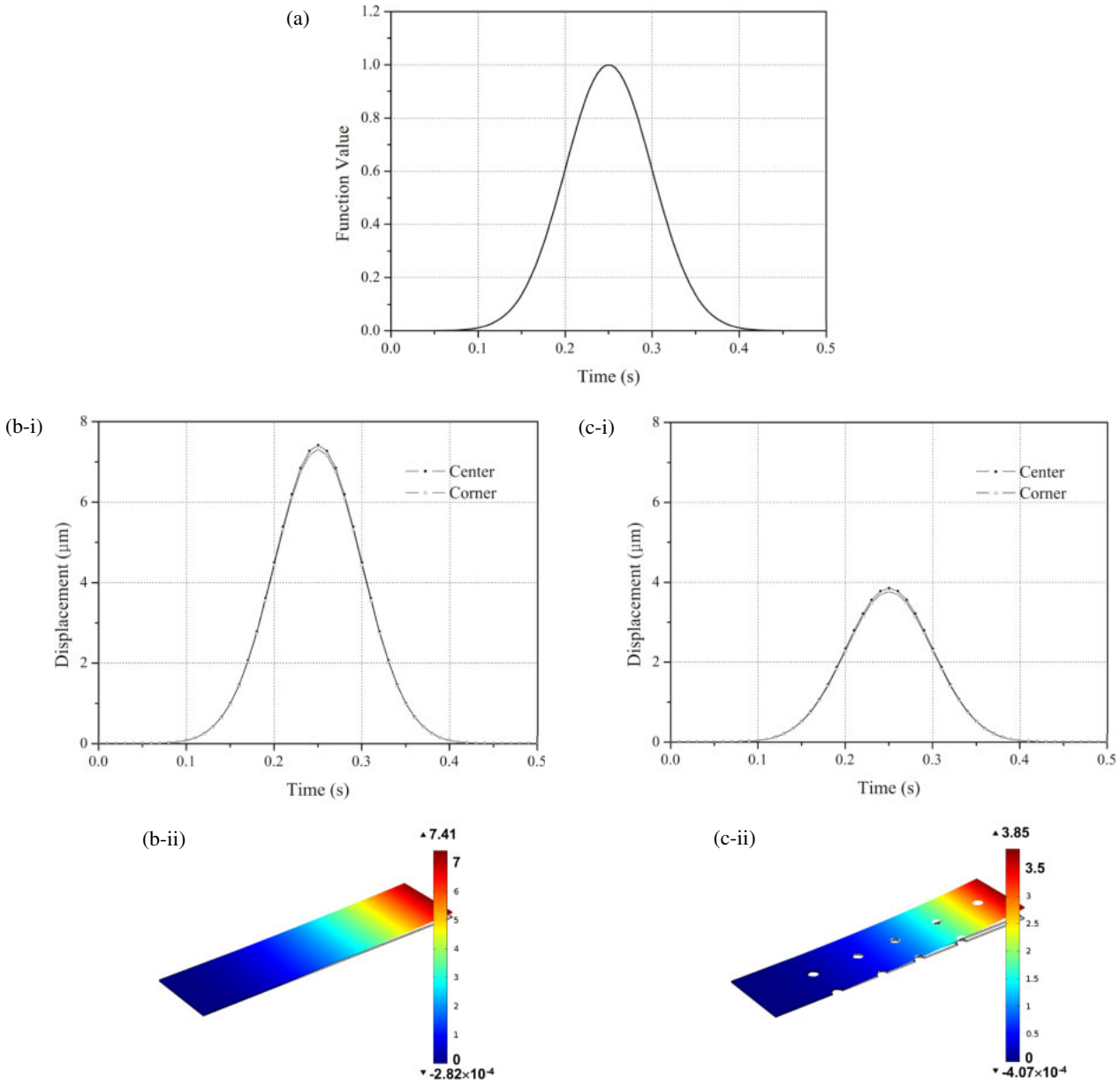

Fig. 7. (Color online) Representative numerical results of the transient analysis: (a) normalized Gaussian function with respect to time as the unit function for the time-varying surface traction, (b) displacement changes in representative points and distribution of the maximum displacement at 0.25 s (with a dimension of μm) for the plain microcantilever, and (c) those for the perforated microcantilever.

analysis because the effective strain for all the cases was quite small. In contrast, the displacement was proportional to the inverse of Young's modulus. Because the cultured CMs exist only on the top surface of the microcantilever, the contractile surface traction is applied within a single cell domain. When only a unit volume corresponding to the single cell domain is considered in the entire microcantilever structure, one can easily establish an equivalent model where the bending moments are applied on the two side surfaces instead of the contractile surface traction pair on the top surface. Therefore, an elastic beam bending theory combining bending moment and beam curvature can be applied.[36)]

$$EI\frac{\partial^2 v}{\partial x^2} = M(x) \tag{2}$$

In Eq. (2), E, I, v, and $M(x)$ represent Young's modulus, moment of inertia of the cross-sectional area, vertical displacement, and bending moment, respectively. From Eq. (2), the inverse relationship between the maximum displacement and the equivalent bending moment from the contractile surface traction can be predicted.

3.4 Transient response of microcantilever sensor

The transient response of the microcantilever sensor was investigated. As explained, the symmetrical model based on a half of the full microcantilever was used to reduce the required computational cost. In addition, the time-varying surface traction was assigned as the transient boundary condition on the top surface. Note that the normalized Gaussian function (mean of 0.25 and standard deviation of 0.05) with a period of 0.5 s was used as the unit time-varying function as plotted in Fig. 7(a). By multiplying the maximum surface traction (5 nN/μm^2 in this specific case) and the unit time-varying function together, the transient surface traction could be simply built. Because only one period was considered in the transient numerical analysis, the surface traction was increased to up to 0.25 s and then decreased.

Figure 7(b-i) shows the displacement change of two representative points in the plain microcantilever when the prescribed transient surface traction was imposed. The displacement distribution at 0.5 s is also shown in Fig. 7(b-ii). The maximum displacement, which was almost identical to the displacement in the static analysis, was observed in the center of the free edge. It was found that there was a slight warpage during the bending of the microcantilever because the corners of the microcantilever showed a relatively lower displacement. The transient response of the microcantilever was similar to the Gaussian function, which was used as the unit function for the surface traction. It showed that the mechanical response of the microcantilever directly reflected the transient change in the CMs contractile surface traction. The same result could be obtained from the transient analysis of the perforated microcantilever, as shown in Figs. 7(c-i) and 7(c-ii).

It may be mentioned that the current numerical model can be used to predict the macroscopic behavior of the microcantilever sensors incorporating CMs. The static and transient investigations showed the same maximum displacement, which is mainly determined by the maximum surface traction. In addition to the effects of focal area and stiffness, the transient analysis also confirmed that the surface traction is the most important factor, which should be considered in designing a similar micromechanical devices.

4. Conclusions

In this study, a numerical investigation was carried out to analyze the macroscopic bending behavior of the perforated microcantilever sensor. To efficiently impose the contractile surface traction of CMs on the numerical analysis as the boundary condition, the simple surface traction model was proposed. From the static and transient analyses, it was verified that the current surface traction model can be efficiently used in a numerical investigation of the micromechanical devices incorporating the CMs. The surface traction or the amount of the contractile force of CMs cultured on the surface was found to be the most crucial factor for the macroscopic bending deformation of the microcantilever sensors compared with the stiffness. In addition, the mechanical response of the microcantilever directly reflected the transient change in the CMs' contractile surface traction.

The proposed numerical method was found to be a useful tool for analyzing the macroscopic behavior of the microcantilever sensors. It can also significantly enhance the understanding of the microcantilever's motion correlated with the CMs' contractile force, thereby providing additional valuable information on the accumulated CMs' physiology. Furthermore, the current method can promote the more efficient development of other micromechanical devices based on the same principle by providing the basic design guide.

Acknowledgments

This work was supported by the International Collaborative R&D Program through the Korea Institute for Advancement of Technology grant funded by the Ministry of Trade, Industry and Energy (N0000894) and Basic Science Research Program through the National Research Foundation of Korea (NRF) funded by the Ministry of Science, ICT & Future Planning (NRF-2014R1A1A1008487).

1) T. Kaneko, E. Takizawa, F. Nomura, T. Hamada, A. Hattori, and K. Yasuda, Jpn. J. Appl. Phys. **52**, 06GK06 (2013).
2) J. Park, J. Ryu, S. K. Choi, E. Seo, J. M. Cha, S. Ryu, J. Kim, B. Kim, and S. H. Lee, Anal. Chem. **77**, 6571 (2005).
3) F. Nomura, A. Hattori, H. Terazono, H. Kim, M. Odaka, Y. Sugio, and K. Yasuda, Jpn. J. Appl. Phys. **55**, 06GN07 (2016).
4) A. W. Feinberg, A. Feigel, S. S. Shevkoplyas, S. Sheehy, G. M. Whitesides, and K. K. Parker, Science **317**, 1366 (2007).
5) Y. Tanaka, K. Morishima, T. Shimizu, A. Kikuchi, M. Yamato, T. Okano, and T. Kitamori, Lab Chip **6**, 230 (2006).
6) X. Liu, X. Wang, H. Zhao, and Y. Du, J. Phys.: Conf. Ser. **557**, 012057 (2014).
7) M. L. Rodriguez, B. T. Graham, L. M. Pabon, S. J. Han, C. E. Murry, and N. J. Sniadecki, J. Biomech. Eng. **136**, 051005 (2014).
8) J. You, H. Moon, B. Y. Lee, J. Y. Jin, Z. E. Chang, S. Y. Kim, J. Park, Y.-S. Hwang, and J. Kim, J. Biomech. **47**, 400 (2014).
9) M. Pesl, J. Pribyl, I. Acimovic, A. Vilotic, S. Jelinkova, A. Salykin, A. Lacampagne, P. Dvorak, A. C. Meli, P. Skladal, and V. Rotrekl, Biosens. Bioelectron. **85**, 751 (2016).
10) Y. Zhao and X. Zhang, Sens. Actuators A **125**, 398 (2006).
11) Q. Cheng, Z. Sun, G. Meininger, and M. Almasri, Sens. Actuators B **188**, 1055 (2013).
12) A. G. Rodriguez, S. J. Han, M. Regnier, and N. J. Sniadecki, Biophys. J. **101**, 2455 (2011).
13) K. Kim, R. Taylor, J. Y. Sim, J. Park, J. Norman, G. Fajardo, D. Bernstein, and B. L. Pruitt, Micro Nano Lett. **6**, 317 (2011).
14) S. J. Han, K. S. Bielawski, L. H. Ting, M. L. Rodriguez, and N. J. Sniadecki, Biophys. J. **103**, 640 (2012).
15) J. Park, S.-K. Ryu, J. Kim, J. Cha, J. Baek, S. Park, B. Kim, and S. H. Lee, J. Biomech. **40**, 2823 (2007).
16) J. Kim, J. Park, K. Na, S. Yang, J. Baek, E. Yoon, S. Choi, S. Lee, K. Chun, J. Park, and S. Park, J. Biomech. **41**, 2396 (2008).
17) A. W. Feinberg, P. W. Alford, H. Jin, C. M. Ripplinger, A. A. Werdich, S. P. Sheehy, A. Grosberg, and K. K. Parker, Biomaterials **33**, 5732 (2012).
18) T. Wang, N. Hu, J. Cao, J. Wu, K. Su, and P. Wang, Biosens. Bioelectron. **49**, 9 (2013).
19) N. Hu, T. Wang, Q. Wang, J. Zhou, L. Zou, K. Su, J. Wu, and P. Wang, Biosens. Bioelectron. **67**, 146 (2015).
20) F. Nomura, K. Matsuura, A. Hattori, M. Odaka, Y. Sugio, H. Kurotobi, H. Terazono, and K. Yasuda, Jpn. J. Appl. Phys. **54**, 06FN06 (2015).
21) J. Y. Kim, Y.-S. Choi, B.-K. Lee, and D.-W. Lee, Biosens. Bioelectron. **80**, 456 (2016).
22) K. Na, J. Kim, S. Yang, Y. M. Yoon, and E. Yoon, NSTI-Nanotech, 2008, p. 737.
23) N. Q. Balaban, U. S. Schwarz, D. Riveline, P. Goichberg, G. Tzur, I. Sabanay, D. Mahalu, S. Safran, A. Bershadsky, L. Addadi, and B. Geiger, Nat. Cell Biol. **3**, 466 (2001).
24) A. Pustoc'h, J. Ohayon, Y. Usson, A. Kamgoue, and P. Tracqui, Acta Biotheor. **53**, 277 (2005).
25) P. Tracqui, J. Ohayon, and T. Boudou, J. Theor. Biol. **255**, 92 (2008).
26) P. Tracqui and J. Ohayon, Philos. Trans. R. Soc. London, Ser. A **367**, 4887 (2009).
27) A. Gizzi, R. Ruiz-Baier, S. Rossi, A. Laadhari, C. Cherubini, and S. Filippi, *Modeling the Heart and the Circulatory System* (Springer, Cham, 2015) p. 157.
28) T. Kaneko, F. Nomura, and K. Yasuda, Jpn. J. Appl. Phys. **50**, 080220 (2011).
29) A. Kamgoué, J. Ohayon, Y. Usson, L. Riou, and P. Tracqui, Cytometry, Part A **75A**, 298 (2009).
30) J.-H. Ahn, C.-S. Park, and D.-W. Lee, Jpn. J. Appl. Phys. **49**, 06GN01 (2010).
31) T. Namazu, *Reliability of MEMS* (Wiley-VCH, Weinheim, 2008) p. 123.
32) U. Allenstein, S. G. Mayr, and M. Zink, Soft Matter **11**, 5053 (2015).
33) H. Haftbaradaran, S. K. Soni, B. W. Sheldon, X. Xiao, and H. Gao, J. Appl. Mech. **79**, 031018 (2012).
34) H.-L. Lee and W.-J. Chang, Jpn. J. Appl. Phys. **51**, 035202 (2012).
35) S. Bhave, *Mechanical Vibrations Theory and Practice* (Dorling Kindersley, New Delhi, 2010) p. 46.
36) A. C. Ugural and S. K. Fenster, *Advanced Strength and Applied Elasticity* (Prentice-Hall, Upper Saddle River, NJ, 2003) 4th ed., p. 187.

